Large-Signal Transient Analysis of Forward Converter With Active-Clamp Reset

Qiong M. Li, *Member, IEEE*, Fred C. Lee, *Fellow, IEEE*, and Milan M. Jovanović, *Fellow, IEEE*

***Abstract*—The forward converter with the active-clamp reset offers many advantages over the forward converters with other transformer-reset methods. However, during the line and load transients, the maximum magnetizing current of the transformer and the peak voltage of the primary switch are strongly affected by the active-clamp circuit dynamics. As a result, the design of a forward converter with the active-clamp reset cannot be optimized based only on its dc characteristics. Due to the nonlinearity of the circuit, it is very difficult to derive the closed-form equations for the transient response of the active-clamp circuit. In this paper, an average-state-trajectory approach is proposed to analyze the transient behavior so that the trends of the maximum magnetizing current of the transformer and the peak voltage of the primary switch can be easily predicted under worst-case conditions and parameter variations.**

***Index Terms*—Active-clamp, forward converter, large-signal transient.**

I. Introduction

THE forward converter is one of the most popular switching topologies for low and medium power applications. To achieve high efficiency at higher switching frequencies, an active-clamp reset circuit is often applied across the main switch [1]. The function of the active-clamp reset circuit is to provide the flux reset of the core of the power transformer, thus eliminating the need for an additional winding or a dissipative RCD-clamp reset. A number of papers have discussed various design issues that relate to the active-clamp reset mechanism [2]–[7], but no explicit analysis has been presented so far for the large-signal transient response. Since during large-signal transients the active-clamp-circuit dynamics strongly affects the maximum magnetizing current of the transformer and the peak voltage of the primary switch, the design of a forward converter with the active-clamp reset cannot be optimized based only on its dc characteristics.

Even though the peak values of the magnetizing current and the primary switch voltage can be easily obtained for a specific set of circuit parameters by using time-domain simulators, simulations do not offer the insight into the general dynamic behavior in terms of the worst-case scenario. In this paper, an average-state-trajectory approach is used to analyze the transient behavior of the active-clamp circuit during line and load changes. The forward converter with output-voltage feedback control is used to demonstrate the proposed analysis approach. It is shown that in addition to the selection of the transformer parameters and active-clamp capacitance, the control loop bandwidth is a major design parameter that determines the maximum voltage of the main power switch and magnetizing current of the transformer during transients. This paper is focused on analyzing the trends of the maximum magnetizing current of the transformer and the peak voltage of the primary switch under worst-case conditions and parameter variations for the converter with the voltage feedback control. The same approach can be extended to the current mode control. The analysis and design guidelines for the current mode control were presented in [8].

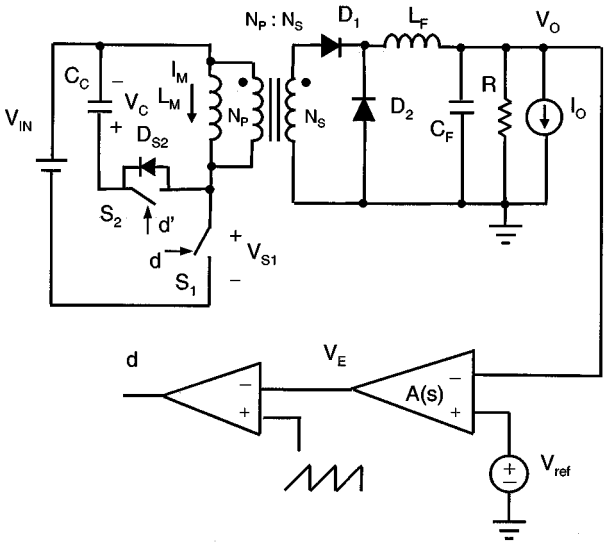

Fig. 1. Circuit diagram of the active-clamp forward converter.

II. Large-Signal Transient Behavior

The forward converter with the active-clamp reset and voltage feedback control is shown in Fig. 1. The active-clamp reset circuit consists of the series connection of auxiliary switch S_2 and clamp capacitor C_C. The transformer in Fig. 1 is modeled as a parallel connection of magnetizing inductance L_M and the ideal transformer with turns ratio $n = (N_P/N_S)$.

To illustrate the behavior of the forward converter with the active-clamp reset, Fig. 2 shows the simulation results of the circuit in Fig. 1 during large-signal transients. Fig. 2(a) shows clamp-capacitor voltage V_C, magnetizing current of the transformer I_M, and output voltage of the error amplifier V_E during

Manuscript received November 25, 1999; revised October 5, 2001. Recommended by Associate Editor F. D. Tan.

Q. M. Li is with Philips Research, Briarcliff Manor, NY 10510 USA (e-mail: michelle_q_li@hotmail.com).

F. C. Lee is with the Virginia Polytechnic Institute and State University, Blacksburg, VA 24061 USA.

M. M. Jovanović is with the Research and Development Department, Delta Products Corporation, Research Triangle Park, NC 27709 USA.

Publisher Item Identifier S 0885-8993(02)02171-3.

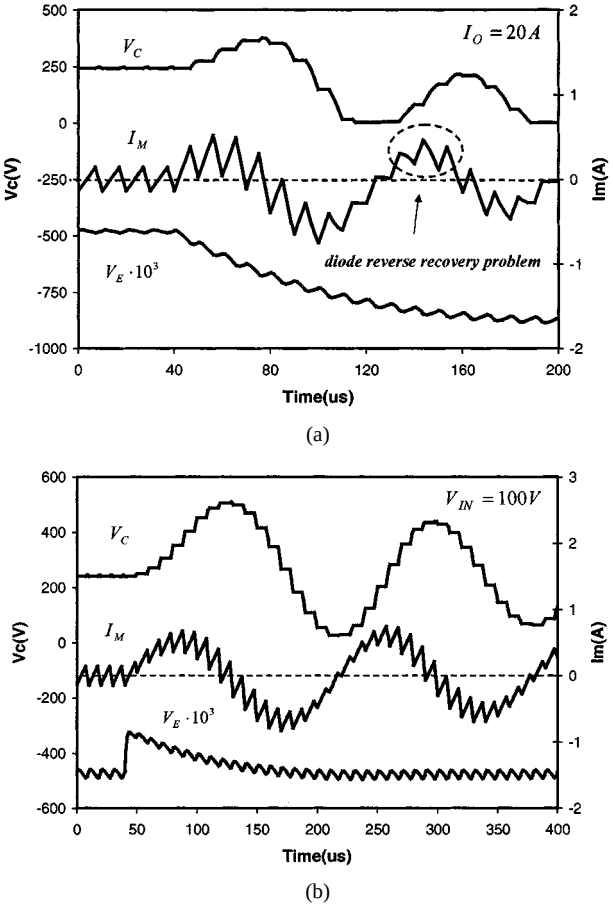

Fig. 2. Simulation results of large-signal transients of the forward converter with the active-clamp reset and output-voltage feedback control: (a) input-voltage step change from 100 V to 200 V and (b) load step change from 18 A to 20 A.

an instantaneous input-voltage transient from 100 V to 200 V. Fig. 2(b) shows the same waveforms during a load transient from 18 A to 20 A. The circuit parameters used in the simulations by using SIMPLIS simulation software [9] are: $L_F = 25$ uH, $C_F = 2000$ uF, $L_M = 2.5$ mH, $C_C = 22$ nF, $n = 11$, maximum duty cycle $D_{\max} = 0.7$, switching frequency $f_s = 100$ kHz, and control-loop crossover frequency $f_c = 3.6$ kHz.

In Fig. 2(a), before the input-voltage transient, the converter operates with a large duty cycle and with a balanced flux in the core of the transformer so that $V_{\rm IN} \cdot D = V_C \cdot (1-D)$. Since after the line change the duty cycle and the clamp-capacitor voltage V_C does not change instantaneously, the volt-second product becomes unbalanced, i.e., $V_{\rm IN} \cdot D > V_C \cdot (1-D)$. As a result, the magnetizing current of the transformer starts increasing after the input-voltage change. The increased magnetizing energy charges the clamp capacitor, increasing the clamp-capacitor voltage. This transition continues until V_C becomes large enough so that the volt-second product becomes $V_{\rm IN} \cdot D < V_C \cdot (1-D)$ and the magnetizing current of the transformer starts to decrease. The described clamp-capacitor voltage increase and the subsequent decrease after the transient can be seen as an oscillatory response of the resonant circuit consisting of the clamp capacitor and the magnetizing inductance of the transformer. Similar resonant behavior during the load transient can be observed in Fig. 2(b).

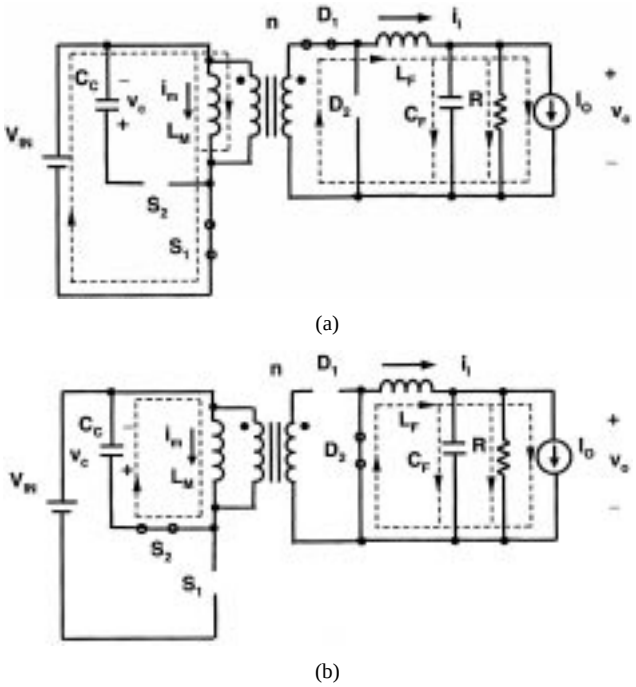

Fig. 3. Simplified circuit diagrams: (a) during the on-period of the main switch and (b) during the off-period of the main switch.

As can be seen from Fig. 2(a) and (b), the peak voltage of the clamp voltage and magnetizing current during transients are much larger than the ripple voltage and current in the steady state. If the forward converter circuit with the active-clamp reset is not correctly designed, the peak clamp-capacitor voltage and magnetizing current during input-voltage and load transients may cause an excessive voltage stress on the primary switch and/or saturation of the core of the transformer. In addition, it may happen that during transients the body diode of auxiliary switch S_2 starts conducting due to a positive magnetizing current at the instant when main switch S_1 is turned on, as indicated in Fig. 2(a). If the auxiliary-switch body diode is conducting when the main switch S_1 is turned on, a slow reverse-recovery of the body diode may cause the failure of the circuit because of the low-impedance current path through the clamp capacitor, the auxiliary-switch body diode, and the main switch [2].

One approach to eliminate this problem is to connect a Schottky diode in series with the auxiliary switch to block the conduction of the body diode and then to connect a fast-recovery anti-parallel diode around the series connection of the Schottky and the auxiliary switch [2]. The other approach is to design an active-clamp circuit so that the magnetizing current is always negative at the instant main switch S_1 is turned on. Therefore, for a proper design of the circuit, it is very important to understand the circuit performance and predict the maximum stresses of the components during large-signal transients.

III. State Trajectory of Active-Clamp Reset Circuit

Fig. 3(a) and (b) are the simplified circuit diagrams of the forward converter with the active-clamp reset during the turn-on and turn-off period of main switch S_1, respectively. According

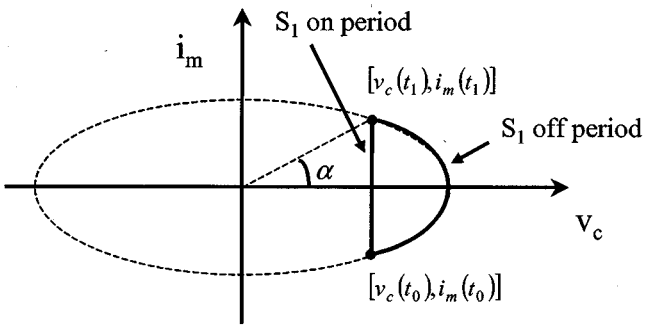

Fig. 4. State trajectory of the active-clamp reset circuit in steady state.

to Fig. 3(a), the state equations of v_c and i_m during the on the period of S_1 are

$$C_C \cdot \frac{dv_c}{dt} = 0 \tag{1}$$

$$L_M \cdot \frac{di_m}{dt} = V_{\text{in}}. \tag{2}$$

By solving (1) and (2), the state trajectory during the on time of S_1 can be described as

$$v_c(t) = v_c(t_0) \tag{3}$$

$$i_m(t) = \frac{V_{\text{in}}}{L_M} \cdot t + i_m(t_0) \tag{4}$$

where $v_c(t_0)$ is the initial value of the clamp-capacitor voltage and $i_m(t_0)$ is the initial value of the magnetizing current of the transformer at the turn-on instant of main switch S_1. The state trajectory during this period is a line parallel to i_m axis with a constant v_c, as shown in Fig. 4.

From Fig. 3(b), during the off period the state equations of v_c and i_m are

$$C_C \cdot \frac{dv_c}{dt} = i_m \tag{5}$$

$$L_M \cdot \frac{di_m}{dt} = -v_c. \tag{6}$$

By solving (5) and (6), the state trajectory during the off time of S_1 can be described as

$$v_c(t) = r \cdot \cos[\alpha - \omega_o(t) \cdot t] \tag{7}$$

$$i_m(t) \cdot Z_o = r \cdot \sin[\alpha - \omega_o(t) \cdot t] \tag{8}$$

$$v_c(t)^2 + [i_m(t) \cdot Z_o]^2 = r^2 \tag{9}$$

where

$$r = \sqrt{v_c(t_1)^2 + i_m(t_1)^2 \cdot Z_o^2} \tag{10}$$

$$\alpha = \tan^{-1}\left(\frac{i_m(t_1) \cdot Z_o}{v_c(t_1)}\right) \tag{11}$$

$$\omega_o = \frac{1}{\sqrt{L_M \cdot C_C}} \tag{12}$$

$$Z_o = \sqrt{\frac{L_M}{C_C}} \tag{13}$$

and $v_c(t_1)$ is the initial value of the clamp-capacitor voltage and $i_m(t_1)$ is the initial value of the magnetizing current of the transformer at the turn-off instant of main switch S_1. The state trajectory during this period is shown in Fig. 4.

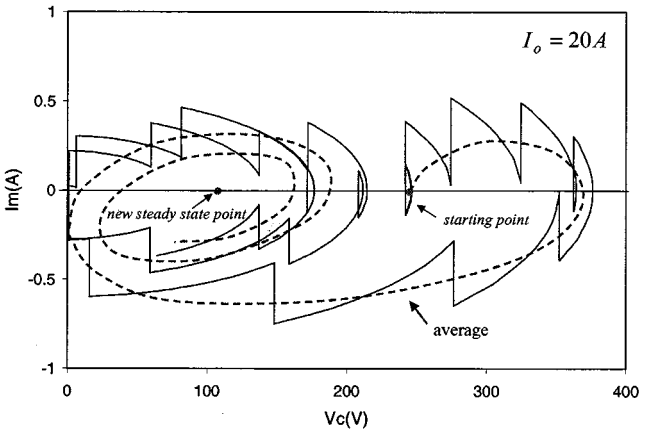

Fig. 5. State trajectory of the active-clamp reset circuit during input-voltage step from 100 V to 200 V transient.

IV. Duty Cycle Equations During Step Input-Voltage and Load Transients

The transient behavior of the active-clamp reset circuit depends on the speed of the control and the characteristics of the resonant circuit. As can be seen from Fig. 2(a) and (b), the clamp voltage and magnetizing current transient waveforms show a resonant behavior with superimposed high switching-frequency ripples. Usually the resonant frequency is much smaller than the switching frequency in order to obtain a small ripple voltage of the clamp capacitor in steady state. Therefore, to simplify the analysis, the switching frequency ripples are ignored in the following analysis. However, the clamp voltage and magnetizing current ripples can be easily added later into the results obtained by the simplified model.

As an illustration, Fig. 5 shows the relationship between a state trajectory (solid line) and an average state trajectory (dashed line) of the active-clamp reset circuit during input- voltage step from 100 V to 200 V transient as in Fig. 2(a). The state trajectory starts with a closed circle as described in Fig. 4. The dashed line shows the average-model state trajectory, which has a simpler waveform. The average state trajectory will be discussed below.

A. Average Model of the Active-Clamp Forward Converter

From Fig. 3(a) and (b), by neglecting the high switching frequency ripples, the average model of the active-clamp forward converter can be written as

$$C_F \cdot \frac{dv_o}{dt} = i_l - I_o - \frac{v_o}{R} \tag{14}$$

$$L_F \cdot \frac{di_l}{dt} = \frac{d \cdot V_{\text{in}}}{n} - v_o \tag{15}$$

$$L_M \cdot \frac{di_m}{dt} = d \cdot V_{\text{in}} - d' v_c \tag{16}$$

$$C_C \cdot \frac{dv_c}{dt} = d' \cdot i_m \tag{17}$$

where d is the duty cycle of main switch and $d' = 1 - d$.

Equations (16) and (17) can be rewritten as

$$\left(\frac{L_m}{d'}\right) \cdot \frac{di_m}{dt} = \frac{d}{d'} \cdot V_{\text{in}} - v_c \tag{18}$$

$$\left(\frac{C_c}{d'}\right) \cdot \frac{dv_c}{dt} = i_m. \tag{19}$$

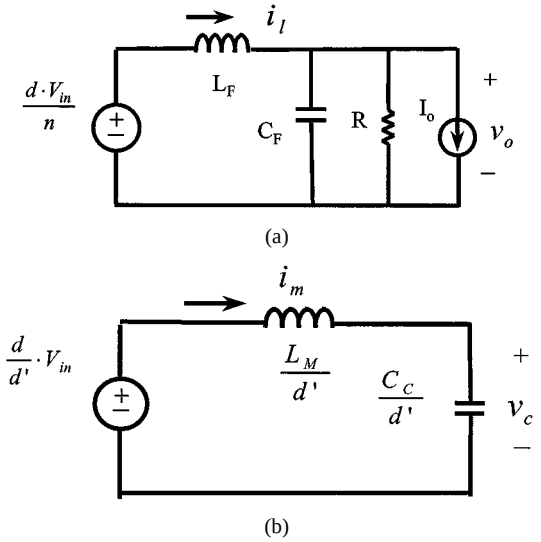

Fig. 6. Average model of the active-clamp forward converter: (a) average model of the forward converter power stage and (b) average model of the active-clamp reset circuit.

According to (14)–(19), the average model of the forward converter power stage and the active-clamp reset circuit can be drawn as in Fig. 6(a) and (b), respectively. As can be seen from Fig. 6, the forward converter power stage and the active-clamp reset circuit are only coupled through the duty cycle. For step input-voltage and load changes, the forward converter power stage represents a linear system. However, the average active-clamp reset circuit is nonlinear with respect to the duty cycle.

B. Duty Cycle Equations During Line and Load Changes

To further study the transient behavior of the active-clamp circuit, it is necessary to find the duty cycle dependence during input-voltage and load changes. Assuming that the input-voltage perturbation is limited to a step change, the following relationships can be established:

$$\begin{aligned} V_{\text{in\_new}} &= V_{\text{in\_old}} + \Delta v_{\text{in}} \\ I_{o\_\text{new}} &= I_{o\_\text{old}} + \Delta i_o \\ D_{\text{new}} &= D_{\text{old}} + \Delta d \\ V_{o\_\text{new}} &= V_{o\_\text{old}} + \Delta v_o \end{aligned} \tag{20}$$

where Δv_{in} and Δi_o are the perturbations and Δd and Δv_o are the corresponding changes.

The perturbations of (14) and (15) yield

$$\Delta v_o = G_d \cdot \Delta d + G_v \cdot \Delta v_{\text{in}} + Z_o \cdot \Delta i_o \tag{21}$$

where

$$G_v = \frac{\Delta v_o}{\Delta v_{\text{in}}} = \frac{\frac{D_{\text{old}}}{n}}{1 + s \cdot \frac{L_F}{R} + s^2 \cdot L_F \cdot C_F} \tag{22}$$

$$Z_o = \frac{\Delta v_o}{\Delta i_o} = -\frac{s \cdot L}{1 + s \cdot \frac{L}{R} + s^2 \cdot L \cdot C} \tag{23}$$

$$G_d = \frac{\Delta v_o}{\Delta d} = \frac{\frac{V_{\text{in\_new}}}{n}}{1 + s \cdot \frac{L_F}{R} + s^2 \cdot L_F \cdot C_F} \tag{24}$$

and D_{old} is the duty cycle before perturbation, $V_{\text{in\_new}}$ is the input voltage after the line step change. The derivations assume

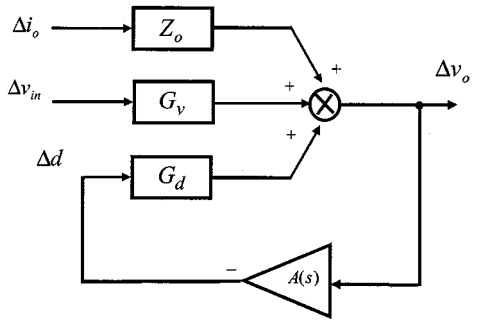

Fig. 7. Forward converter closed-loop block diagram.

that at the instant of the input step change the new input voltage is $V_{\text{in\_new}}$, whereas the new duty cycle is still D_{old} since the duty cycle cannot be changed instantaneously.

As shown in the closed-loop block diagram of the forward converter in Fig. 7, assuming that the transfer function of control loop compensator is $A(s)$, the loop gain is $T(s) = A(s) \cdot G_d(s)$. According to Fig. 7, the closed-loop equations are

$$\left.\frac{\Delta d}{\Delta v_{\text{in}}}\right|\text{close} = \frac{\Delta d}{\Delta v_o} \cdot \frac{\Delta v_o}{\Delta v_{\text{in}}} = -\frac{D_{\text{old}}}{V_{\text{in\_new}}} \cdot \frac{T(s)}{1+T(s)} \tag{25}$$

$$\left.\frac{\Delta d}{\Delta i_o}\right|\text{close} = \frac{\Delta d}{\Delta v_o} \cdot \frac{\Delta v_o}{\Delta i_o} = \frac{s \cdot L_F \cdot n}{V_{\text{in\_new}}} \cdot \frac{T(s)}{1+T(s)}. \tag{26}$$

Generally, neglecting the ESR zero of output-filter capacitor C_F, the optimal compensation of the output-voltage feedback control loop requires the transfer function of the compensator in the form

$$A(s) = \frac{A_{\text{dc}}}{s} \cdot \frac{(1 + s/\omega_{z1}) \cdot (1 + s/\omega_{z2})}{(1 + s/\omega_p)} \tag{27}$$

where, compensator zeroes ω_{z1} and ω_{z2} are placed to cancel two poles in G_d transfer function, i.e., ω_{z1} and ω_{z2} are close to $(1/\sqrt{L_F \cdot C_F})$, and ω_p is placed at a frequency between crossover frequency ω_c and switching frequency ω_s [10].

Since when $T \gg 1, (T)/(1+T) \approx 1$, and when $T \ll 1, (T)/(1+T) \approx T$. The $(T)/(1+T)$ transfer function becomes

$$\frac{T}{1+T} \approx \frac{1}{(1 + s/\omega_c) \cdot (1 + s/\omega_p)} \tag{28}$$

as shown in Fig. 8.

Substituting (28) into (25) and (26), the closed-loop transfer functions are

$$\left.\frac{\Delta d}{\Delta v_{\text{in}}}\right|_{\text{close}} = -\frac{D_{\text{old}}}{V_{\text{in\_new}}} \cdot \frac{1}{(1 + s/\omega_c) \cdot (1 + s/\omega_p)} \tag{29}$$

$$\left.\frac{\Delta d}{\Delta i_o}\right|_{\text{close}} = \frac{s \cdot L_F \cdot n}{V_{\text{in\_new}}} \cdot \frac{1}{(1 + s/\omega_c) \cdot (1 + s/\omega_p)}. \tag{30}$$

Therefore, from (29), for a step input-voltage change, the time domain equation for the duty cycle can be written as

$$d(t) = D_{\text{old}} + (D_{\text{new}} - D_{\text{old}}) \cdot \left(1 - \frac{\omega_p}{\omega_p - \omega_c} e^{-\omega_c \cdot t} + \frac{\omega_c}{\omega_p - \omega_c} e^{-\omega_p \cdot t}\right). \tag{31}$$

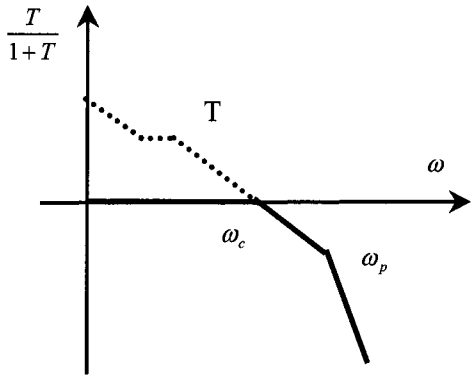

Fig. 8. Bode plot of $T/(1+T)$.

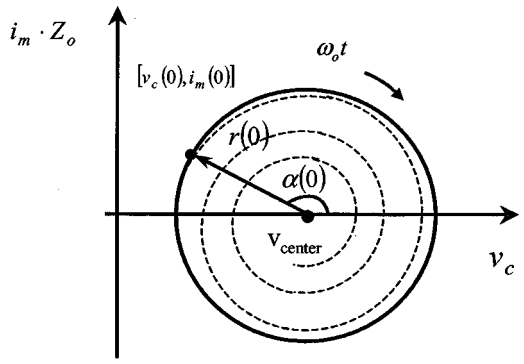

Fig. 9. Average state trajectory without damping (solid line) and with damping (dashed line).

Because generally ω_p is selected so that $\omega_p \gg \omega_c$, (31) can be simplified to

$$d(t) \approx D_{\text{old}} + (D_{\text{new}} - D_{\text{old}}) \cdot (1 - e^{-\omega_c \cdot t}). \quad (32)$$

Similarly, from (30), under the same assumptions, the time domain equation for the duty cycle during a step load change can be obtained as

$$d(t) = D_{\text{old}} + \frac{n \cdot \omega_c \cdot L_F}{V_{\text{in}}} \cdot \Delta I_o \cdot e^{-\omega_c \cdot t}. \quad (33)$$

V. Large-Signal Transient Analysis

A. Average State Trajectory Equations

From Fig. 6, it can be seen that the average model of the active-clamp reset circuit is a nonlinear system whose parameters are the functions of the duty cycle. At the same time, the duty cycle is independent of the parameters of the L_M-C_C resonant network, i.e., it is decoupled from the state variables, v_c and i_m. In addition, since the duty cycle does not change during a switching period (sampling nature of PWM), the average model in Fig. 6(b) can be considered linear during each switching period with input voltage fixed at $(d/d') \cdot V_{\text{in}}$, magnetizing inductance fixed at (L_M/d'), and clamp capacitance fixed at (C_C/d').

By solving (18) and (19), the state trajectory equations during each switching period are

$$v_c(t) = r(0) \cdot \cos[\alpha(0) - \omega_o \cdot t] + v_{\text{center}} \quad (34)$$

$$i_m(t) \cdot Z_o = r(0) \cdot \sin[\alpha(0) - \omega_o \cdot t] \quad (35)$$

where

$$v_{\text{center}} = \frac{d}{d'} \cdot V_{\text{in}}, \quad (36)$$

$$r(0) = \sqrt{[v_c(0) - v_{\text{center}}(0)]^2 + i_m(0)^2 \cdot Z_o^2}, \quad (37)$$

$$\alpha(0) = \tan^{-1}\left(\frac{i_m(0) \cdot Z_o}{v_c(0) - v_{\text{center}}}\right). \quad (38)$$

In (34)–(38), $v_C(0)$ is the initial average voltage of the clamp capacitor, $i_m(0)$ is the initial average magnetizing current of the transformer, $\omega_o = (d'/\sqrt{L_M \cdot C_C})$ is the resonant frequency of L_M-C_C resonant network, and $Z_o = \sqrt{L_M/C_C}$ is the characteristic impedance of the resonant network.

By combining (34) and (35), the averaged state trajectory equation can be written as

$$[v_c(t) - v_{\text{center}}]^2 + [i_m(t) \cdot Z_o]^2 = r(0)^2. \quad (39)$$

The average state trajectory is an ellipse with center $(v_{\text{center}}, 0)$ in the $v_c - i_m$ state plane, and a circle in the $v_c - i_m \cdot Z_o$ state plane as shown with the solid line in Fig. 9. The dynamic equilibrium point, v_{center}, is the center of the state trajectory and is a function of the duty cycle and input voltage.

Because the duty cycle is a slow varying variable compared with a switching period, duty cycle $d(t)$ changes gradually during a transient. Consequently, it can be assumed that the average state trajectory movement is a continuous movement with moving center $v_{\text{center}}(t)$ described by equations (34)–(39), where all quantities dependent on duty cycle are functions of time.

Similarly, one can analyze the average state trajectory in the presence of resistive loss R_M which represents a sum of the switch on resistance and the core loss of the transformer. The normalized average state trajectory with damping R_M is shown with a dashed line in Fig. 9. v_{center} is the spiral point of the state trajectory and the damping of the trajectory is $e^{-(R_M/2 \cdot L_M) \cdot t}$. Since the time constant in the damping term is usually very large when no external damping circuit is used, the effect of the damping does not have a significant impact on peak values of state variables in the transient analysis. The rest of the paper will analyze the circuit's transient behavior without the damping effect.

B. Movement of the Average State Trajectory During Input-Voltage Transient

Before the input-voltage step change from $V_{\text{in\_old}}$ to $V_{\text{in\_new}}$, the average state trajectory is a single point in the $v_c - i_m \cdot Z_o$ state plane with duty cycle $d = D_{\text{old}}$, initial average clamp-capacitor voltage $v_c(0) = (D_{\text{old}}/D'_{\text{old}}) \cdot V_{\text{in\_old}}$, and the average magnetizing current of the transformer $i_m(0) = 0$. Since immediately after an input-voltage step change, the duty cycle cannot change instantaneously, the trajectory center after the change is $v_{\text{center}}(0) = (D_{\text{old}}/D'_{\text{old}}) \cdot V_{\text{in\_new}}$ and the average state trajectory follows the circle described in (39) with the center $[v_{\text{center}}(0), 0]$ and radius $r(0) = |v_{\text{center}}(0) - v_c(0)|$. Since a larger duty cycle has a larger $v_{\text{center}}(0)$ and $v_c(0)$, thus higher peak clamp-capacitor voltage and magnetizing current of

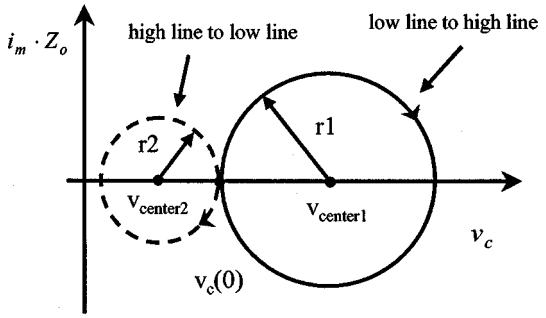

Fig. 10. Open-loop state trajectories during input step changes.

the transformer during input-step changes, a circuit with larger $D_{\max}$ typically has higher stresses.

When the converter operates with the control loop open, i.e., has a fixed duty cycle, d does not change. Consequently, v_{center} and r do not change, and the state trajectory is a fixed circle as shown in Fig. 10. However, when the forward converter has an output-voltage feedback control, the duty cycle changes gradually from D_{old} to D_{new} as described in (32) so the center of the circle moves from $v_{\text{center}}(0)$ to $v_{c\_\text{new}} = (D_{\text{new}}/D'_{\text{new}}) \cdot V_{\text{in\_new}}$, which is the new steady state value of the clamp-capacitor voltage. The trajectory movement is illustrated in Fig. 11.

Fig. 11(a) and (b) are the state trajectories during input-voltage from 200 V to 300 V transient with a bandwidth $f_c = 3$ kHz and $f_c = 20$ kHz, respectively. Both state trajectories follow the open loop circle (dashed line) at the beginning of the transient. Since v_{center} moves faster in Fig. 11(b) due to a higher bandwidth, the state trajectory takes less time to move to the new steady state, which results in a lower peak voltage of the switch and a lower peak magnetizing current (smaller thick solid-line circle).

Fig. 11(c) and (d) are the state trajectories during input-voltage from 300 V to 200 V transient with a bandwidth $f_c = 3$ kHz and $f_c = 20$ kHz, respectively. These trajectories are similar to those observed in Fig. 11(a) and (b). As can be seen from Fig. 11, the worst case (largest thick solid-line circle) happens when the input-voltage steps from low to high, and the bandwidth is the lowest.

From the state trajectory analysis, we can see that the resonant frequency of the active-clamp circuit plays an important role, since the state trajectory is determined by two movements, the state trajectory center movement, whose speed is controlled by bandwidth f_c and the resonant movement, whose speed is determined by resonant frequency f_o. Fig. 12 shows the normalized maximum average v_c and i_m as a function of f_o/f_c for line transient. In Fig. 12, the input-voltage-step changes instantaneously from $V_{\text{in\_min}}$ to 200% $V_{\text{in\_min}}$, whereas $D_{\max=0.7}$ For the same bandwidth, a lower resonant frequency has a smaller peak clamp-capacitor voltage and peak magnetizing current.

The peak magnetizing current of the transformer $i_m(\text{peak})$ and the peak voltage of the main switch $v_{s1}(\text{peak})$ can be calculated by adding the ripples as

$$i_m(\text{peak}) = i_{m\_\text{ave}}(\max) + \frac{1}{2} \cdot \frac{V_{\text{in}} \cdot D \cdot T_s}{L_M} \tag{40}$$

$$v_{s1}(\text{peak}) = V_{\text{in\_new}} + v_{c\_\text{ave}}(\max) + \frac{1}{2} \cdot \frac{1}{8} \cdot \frac{D' \cdot n \cdot V_o \cdot T_s^2}{L_M \cdot C_C} \tag{41}$$

where $i_{m\_\text{ave}}(\max)$ is the maximum magnetizing current of the transformer and $v_{c\_\text{ave}}(\max)$ is the maximum voltage of the clamp capacitor in the average stage trajectory, and D is somewhere between D_{old} and D_{new}. For the worst-case scenario, (40) should be calculated for the larger value of D_{old} and D_{new}, whereas (41) should be calculated for the smaller value of D_{old} and D_{new}. The values of $i_{m\_\text{ave}}(\max)$ and $v_{c\_\text{ave}}(\max)$ can be calculated by simulating the average model of the active-clamp forward converter shown in Fig. 6 under worst-case conditions.

C. Movement of State Trajectory During Load Transient

Before a load step change, the average state trajectory is a single point in the $v_c - i_m \cdot Z_o$ state plane with duty cycle $d = D_{\text{old}}$, initial average clamp-capacitor voltage $v_c(0) = (D_{\text{old}}/D'_{\text{old}}) \cdot V_{\text{in}}$ and the average magnetizing current of the transformer $i_m(0) = 0$. According to (33), at the moment of a step load change, the duty cycle changes to

$$\Delta d = \frac{n \cdot \omega_c \cdot L_F}{V_{\text{in}}} \cdot \Delta I_o, \tag{42}$$

so that the initial trajectory center is

$$v_{\text{center}}(0) = \frac{D_{\text{old}} + \Delta d}{D'_{\text{old}} - \Delta d} \cdot V_{\text{in}}. \tag{43}$$

The average state trajectory follows the circle described in (39) with the circle center at $[v_{\text{center}}(0), 0]$ and the radius $r(0) = |v_{\text{center}}(0) - v_c(0)|$. Since a larger duty cycle has a larger $v_{\text{center}}(0)$ and $v_c(0)$, thus higher peak clamp-capacitor voltage and magnetizing current of the transformer during load transients, a circuit with larger $D_{\max}$ typically has higher stresses.

Because of the output-voltage feedback control, the duty cycle returns gradually to D_{old} as described in (33). Therefore, the center of the circle moves from $v_{\text{center}}(0)$ to $v_c(0)$, which is the original steady state value of the clamp-capacitor voltage, as illustrated in Fig. 13.

Fig. 13(a) and (b) are the state trajectories during a step-load change from 18 A to 20 A with a bandwidth of $f_c = 700$ Hz and $f_c = 7$ kHz, respectively. The f_o in the figure is 21.5 kHz. Both state trajectories follow the open loop circle (dashed line) at the beginning of the transient. Since v_{center} moves faster in Fig. 13(b) due to a higher bandwidth, the state trajectory takes less time to move to the new steady state. It should be noted that according to (33), the circuit with higher control bandwidth has a larger initial duty cycle jump. As a result, the initial radius $r(0)$ is much larger for the high bandwidth case. This is the opposite of the case of a step input-voltage change, where the circuit with a lower bandwidth control experiences a larger maximum clamp-capacitor voltage and magnetizing current.

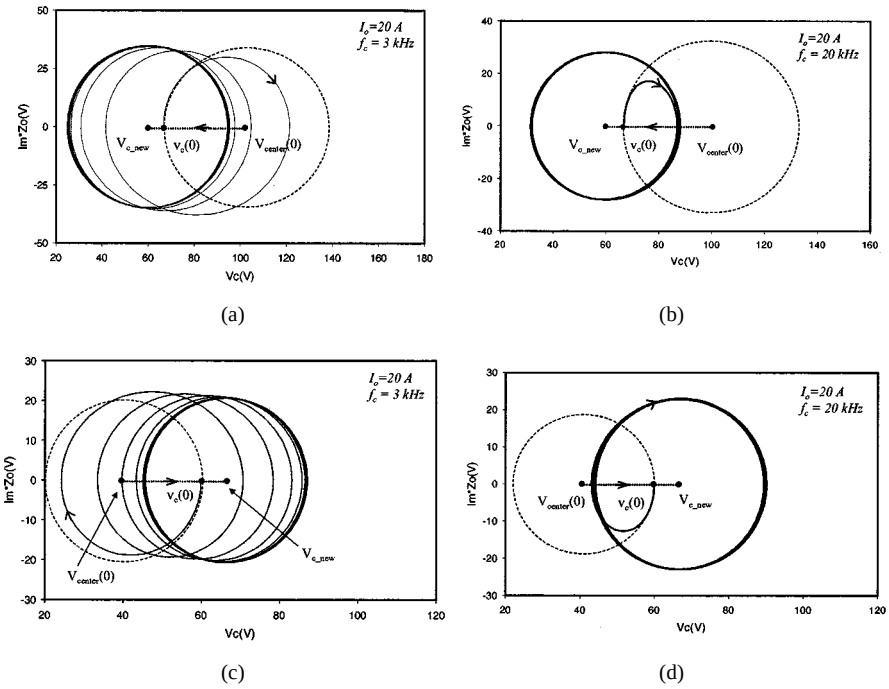

Fig. 11. Closed-loop average state trajectories with different bandwidths and input step changes: (a)–(b) input-voltage step from 200 V to 300 V; (c)–(d) input-voltage step from 300 V to 200 V.

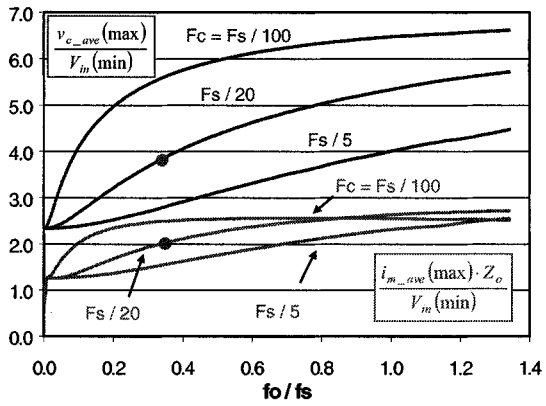

Fig. 12. Normalized maximum average v_c and i_m as a function of f_o/f_c for line transient.

Fig. 13(c) and (d) show the state trajectories during a step-load change from 20 A to 18 A with a bandwidth of $f_c = 700$ Hz and $f_c = 7$ kHz, respectively. As can be seen from Fig. 13, the maximum transient voltage stress of the switch and the maximum transient magnetizing current occur for a positive step-load change with a high bandwidth. For the same bandwidth, a lower resonant frequency has a smaller peak clamp-capacitor voltage and peak magnetizing current.

Generally, the minimum input-voltage condition exhibits the largest clamp-capacitor voltage and the magnetizing current transient since $v_{\text{center}}(0)$ is the largest due to the smallest d'. A smaller output-filter inductance helps to reduce the duty cycle change during transients and reduces the peak voltage and the magnetizing current. Fig. 14 shows the normalized maximum average v_c and i_m as a function of f_o/f_c for the load transient. The load step changes are from 90% of full load to full load, whereas $D_{\max} = 0.7$.

VI. Experimental Verification

The presented analysis was verified on a 100 W, 5 V forward converter with active clamp reset circuit shown in Fig. 15. The input-voltage range of the circuit is 40–100 V, the switching frequency is 100 kHz, and the maximum duty cycle is 0.7. As shown in Fig. 15, the magnetizing inductance is 1 mH and the clamp capacitance is 22 nF. The control bandwidth is 2 kHz.

Fig. 16 shows the experimental waveforms of the clamp capacitor, V_C, and the magnetizing current, I_M for an input step change from 50 to 75 V with 10 A load. Fig. 17 shows the measured (solid line) average state trajectories of V_C and I_M and the corresponding calculated (dashed line) trajectories using the model without damping. The average state trajectories are generated by moving-averaging of the measured data. As can be seen from Fig. 17, the measured V_C and I_M reach the new steady state faster than the calculated due to the damping in the real circuit. Nevertheless, the model without damping predicts very well the peak clamp capacitor voltage and the peak magnetizing current during the line transient and, consequently, it is quite adequate for the worst-case analysis and design purposes.

Fig. 18 shows the experimental waveforms of the clamp capacitor, V_C, and the magnetizing current, I_M with a load step change from 10 to 15 A for the input voltage of 50 V. Fig. 19 shows the calculated (dashed line) and measured (solid line) average state trajectories of V_C and I_M. Similarly, as for the input-voltage step change, the measured V_C and I_M reach the

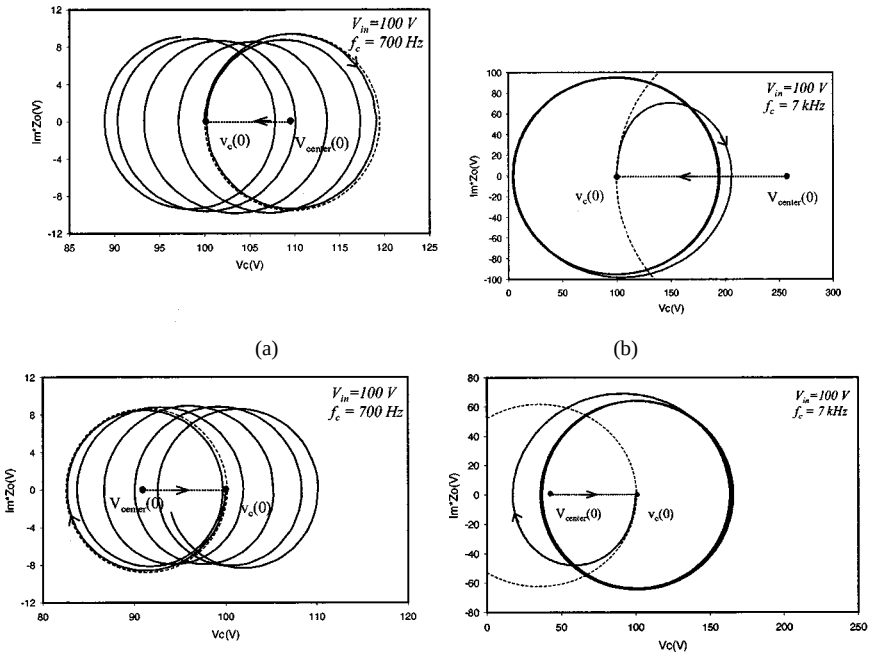

Fig. 13. Closed-loop average state trajectories with different control bandwidths and load step changes: (a)–(b) load current step from 18 A to 20 A; (c)–(d) load current step from 20 A to 18 A.

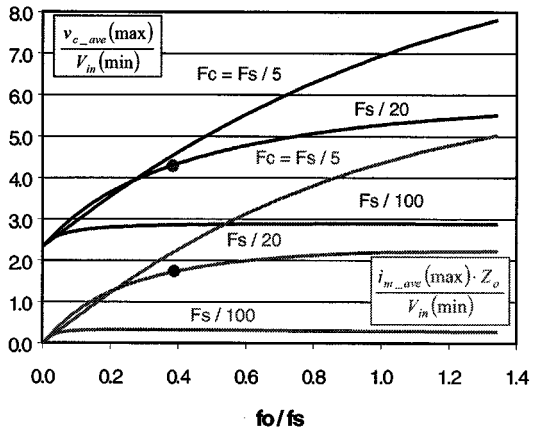

Fig. 14. Normalized maximum average v_c and i_m as a function of f_o/f_c for the load transient. The load step changes are from 90% of full load to full load, whereas $D_{\max} = 0.7$.

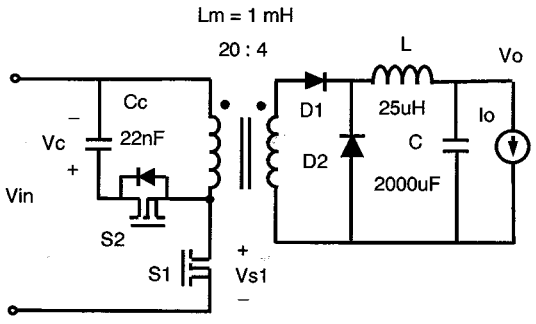

Fig. 15. Circuit diagram of the experimental circuit.

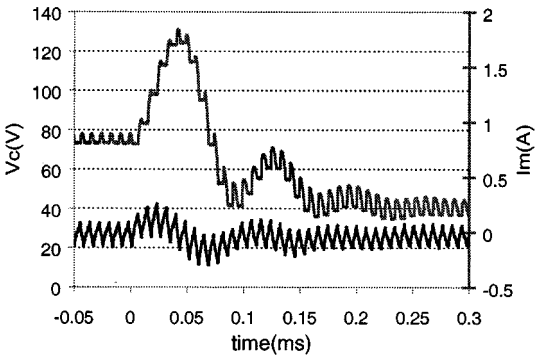

Fig. 16. Experimental waveforms with input step change from 50 V to 75 V: Time domain waveforms of clamp capacitor voltage and magnetizing current.

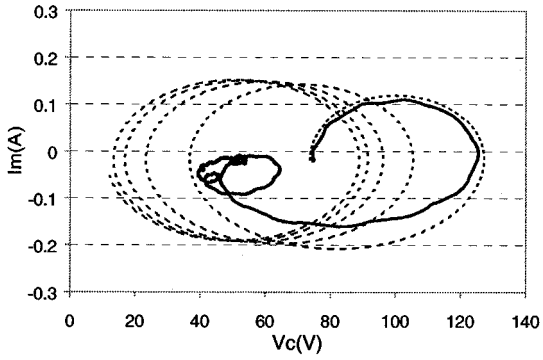

Fig. 17. Comparison of calculated (dashed line) and measured (solid line) averaged state trajectories of V_C and I_M during 50–75 V input-voltage transient.

new steady state faster than the calculated due to the damping in the real circuit. However, the analysis also predicts the dynamics of the peak clamp capacitor voltage and the peak magnetizing current very well during the load transient.

VII. Design Considerations

Generally, because of the EMI input filter, any line voltage transient will be slowed down at the input of the forward converter, i.e., the slope of the voltage transient will be reduced.

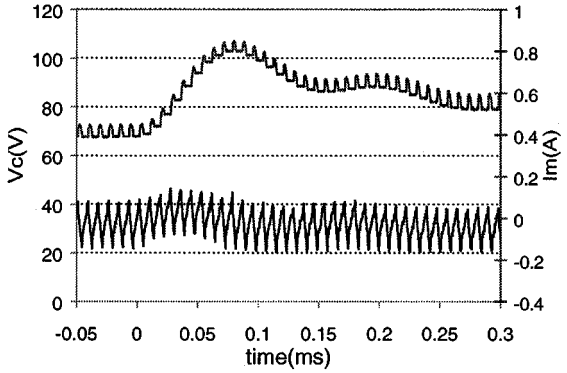

Fig. 18. Experimental waveforms with load step change from 10 A to 15 A: Time domain waveforms of clamp capacitor voltage and magnetizing current.

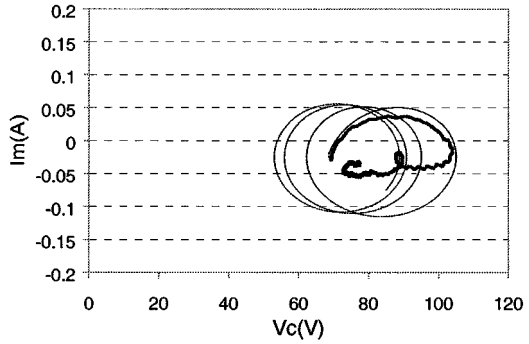

Fig. 19. Comparison of calculated (dashed line) and measured (solid line) averaged state trajectories of V_C and I_M during 10–15 A load transient.

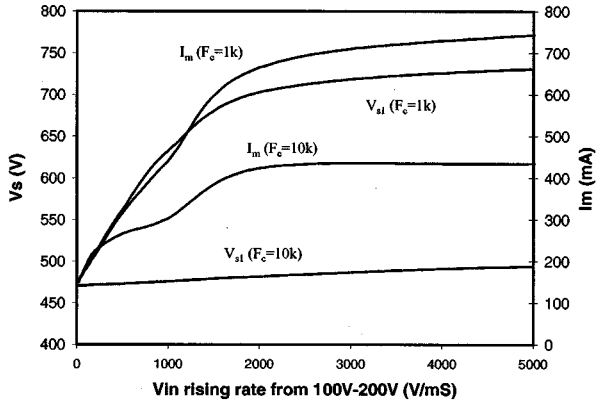

Fig. 20. Maximum switch voltage and magnetizing current with different input voltage rising rates.

This reduced slope change also reduces the peak voltage of the switch and the magnetizing current as shown in Fig. 20. In Fig. 20, the input changes from 100 V to 200 V with different rising rates. In off-line applications with a rectifier circuit as the input source to the forward converter, assuming that 115 $V_{\rm AC}$ input voltage recovers from a -30% sag, the input voltage of the active-clamp converter will have an approximately 100–200 V slope change within 5 ms. This corresponds to 20 V/mS rising rate. Fig. 20 shows that with this low rising rate, the circuit does not have any transient problem.

If the circuit experiences a faster line transient, e.g., under some abnormal condition, it could have problems when the rising rate exceeds a critical value, e.g., the critical value is 700 V/mS in a forward converter with $F_c = 1$ kHz using 600 V voltage-rating device. One possible solution to this problem is to add a voltage feed-forward limit in the control design to reduce the initial radius $r(0)$, and thus having a smaller peak clamp capacitor voltage and magnetizing current.

During load transients, the rising rate can be much faster than the one in the line transient, so the compensator could be saturated at the beginning of the transient. In this case, the duty cycle will be clamped to the maximum clamp value for a period of time until the circuit recovers to the normal operation. It is relatively easy to enhance the circuit's transient performance from high load to low load because the control can be implemented so that the gate signal of the clamp switch is shut down when the duty cycle becomes zero [4]. For transients from low load to high load one can see from (43) that $v_{\rm center}(0)$ becomes extremely large with a duty cycle close to 1 (e.g., 90%), producing an excessive transient peak voltage and magnetizing current. Therefore, the major design challenge is to keep the peak switch voltage and magnetizing current within the permissible limits during low-load to high-load transients. The design trade-offs are discussed and the detailed design guidelines are given in [8].

VIII. Summary

An average-state-trajectory approach is proposed to analyze the forward converter with the active-clamp reset and the output-voltage feedback control. Based on the analysis, the circuit performance during large-signal line and load transients can be predicted. The analysis results match the experimental results very well during both the line and load transients. The worst-case scenarios occur when the input voltage changes from the minimum line voltage to a higher voltage and when the load experiences a low to high change at the minimum line voltage. It is shown that besides the clamp capacitance and the magnetizing inductance of the power transformer, the control bandwidth plays a major role in determining the maximum clamp-capacitor voltage and magnetizing current.

References

[1] P. Vinciarelli, "Optimal resetting of the transformer's core in single ended forward converters," U.S. Patent 4 441 146, Apr. 1984.

[2] B. Carsten, "Design techniques for transformer active reset circuits at high frequencies and power levels," in *Proc. Conf. High Freq. Power Conv.*, 1990, pp. 235–246.

[3] B. Andreycak, "Active clamp and reset technique enhances forward converter performance," in *Proc. Unitrode Power Supply Design Sem., SEM-1000*, 1994, pp. 3-1–3-18.

[4] D. Dalal and L. Wofford, "Novel control IC for single-ended active clamp converters," in *Proc. High Freq. Power Conv. Conf.*, 1995, pp. 136–146.

[5] C. S. Leu, G. Hua, and F. C. Lee, "Comparison of forward topologies with various reset schemes," in *Proc. High Freq. Power Conv. Conf.*, 1992, pp. 198–208.

[6] I. D. Jitaru, "Constant frequency, forward converter with resonant transition," in *Proc. High Freq. Power Conv. Conf.*, 1991, pp. 282–292.

[7] Q. Li, F. C. Lee, and M. M. Jovanović, "Design considerations of transformer DC bias of forward converter with active-clamp reset," *Proc. IEEE APEC'99*, pp. 553–559, Mar. 1999.

[8] Q. Li and F. C. Lee, "Design consideration of the active-clamp forward converter with current mode control during large-signal transient," *Proc. IEEE APEC'00*, pp. 966–972, Feb. 2000.

[9] *SIMPLIS User's Manual*, Sept. 1994. Release 2.5.

[10] F. C. Lee, Z. D. Fang, and T. H. Lee, "Optimal design strategy of switching converters employing current injected control," *IEEE Trans. Aerosp. Electron. Syst.*, vol. AES-21, pp. 21–35, Jan. 1985.

Qiong M. Li (M'99) received the B.S. and M.S. degrees in electrical engineering from Xian Jiaotong University, Xian, China, in 1988 and 1991, respectively, and the Ph.D. degree in electrical and computer engineering from the Center of Power Electronics Systems (CPES), Virginia Polytechnic Institute and State University, Blacksburg, in 1999.

She is a Senior Member of Research Staff, Philips Research USA, Briarcliff Manor, NY, where she is mainly responsible for the research and technology development of digital control systems for power supplies and lighting applications. Her main research interests include power converter analysis and design, digital control system implementation, DSP control algorithms, modeling, and simulation of power converters.

Dr. Li is a member of the IEEE Power Electronics Society, Phi Kappa Phi, and Eta Kappa Nu.

Fred C. Lee (S'72–M'74–SM'87–F'90) received the B.S. degree in electrical engineering from the National Cheng Kung University, Taiwan, R.O.C., in 1968 and the M.S. and Ph.D. degrees in electrical engineering from Duke University, Durham, NC, in 1971 and 1974, respectively.

He is a University Distinguished Professor with Virginia Polytechnic Institute and State University (Virginia Tech), Blacksburg, and prior to that he was the Lewis A. Hester Chair of Engineering at Virginia Tech. He directs the Center for Power Electronics Systems (CPES), a National Science Foundation engineering research center whose participants include five universities and over 100 corporations. In addition to Virginia Tech, participating CPES universities are the University of Wisconsin-Madison, Rensselaer Polytechnic Institute, North Carolina A&T State University, and the University of Puerto Rico-Mayaguez. He is also the Founder and Director of the Virginia Power Electronics Center (VPEC), one of the largest university-based power electronics research centers in the country. VPEC's Industry-University Partnership Program provides an effective mechanism for technology transfer, and an opportunity for industries to profit from VPEC's research results. VPEC's programs have been able to attract world-renowned faculty and visiting professors to Virginia Tech who, in turn, attract an excellent cadre of undergraduate and graduate students. Total sponsored research funding secured by him over the last 20 years exceeds $35 million. His research interests include high-frequency power conversion, distributed power systems, space power systems, power factor correction techniques, electronics packaging, high-frequency magnetics, device characterization, and modeling and control of converters. He holds 19 U.S. patents, and has published over 120 journal articles in refereed journals and more than 300 technical papers in conference proceedings.

Dr. Lee received the Society of Automotive Engineering's Ralph R. Teeter Education Award (1985), Virginia Tech's Alumni Award for Research Excellence (1990), and its College of Engineering Dean's Award for Excellence in Research (1997), in 1989, the William E. Newell Power Electronics Award, the highest award presented by the IEEE Power Electronics Society for outstanding achievement in the power electronics discipline, the Power Conversion and Intelligent Motion Award for Leadership in Power Electronics Education (1990), the Arthur E. Fury Award for Leadership and Innovation in Advancing Power Electronic Systems Technology (1998), the IEEE Millennium Medal, and honorary professorships from Shanghai University of Technology, Shanghai Railroad and Technology Institute, Nanjing Aeronautical Institute, Zhejiang University, and Tsinghua University. He is an active member in the professional community of power electronics engineers. He chaired the 1995 International Conference on Power Electronics and Drives Systems, which took place in Singapore, and co-chaired the 1994 International Power Electronics and Motion Control Conference, held in Beijing. During 1993-1994, he served as President of the IEEE Power Electronics Society and, before that, as Program Chair and then Conference Chair of IEEE-sponsored power electronics specialist conferences.

Milan M. Jovanović (F'01) was born in Belgrade, Yugoslavia. He received the Dipl.Ing. degree in electrical engineering from the University of Belgrade.

Presently, he is the Vice President for Research and Development of Delta Products Corporation, Research Triangle Park, NC (U.S. subsidiary of Delta Electronics, Inc., Taiwan, R.O.C.), one of the world's largest manufacturers of power supplies. His current research is focused on power conversion and management issues of server, telecom, and portable data-processing equipment.